




Symmetry and polarity of antiphase boundaries in PbZrO_3 I. Rychetsky ^{*}*Institute of Physics of the Czech Academy of Sciences, Na Slovance 2, 18221 Prague 8, Czech Republic*W. Schranz  and A. Tröster *University of Vienna, Faculty of Physics, Boltzmanngasse 5, 1090 Wien, Austria*

(Received 16 November 2021; revised 6 December 2021; accepted 7 December 2021; published 23 December 2021)

The polar properties of antiphase boundaries (APBs) in PbZrO_3 are analyzed in detail using a recently developed layer group approach in order parameter (OP) space and compared with the results from Landau-Ginzburg free energy description. It is shown that the former approach reveals the properties of the microscopic APBs and predicts polar APB structures at particular positions inside the unit cell, which agree very well with recent experimental observations [Wei *et al.*, *Nat. Commun.* **5**, 3031 (2014), Wei *et al.*, *Mater. Res. Bull.* **62**, 101 (2015)]. The systematic usage of the method is developed. In contrast with it, the commonly used free energy description obscures the microscopic features but still can reflect the macroscopic properties of the APBs by considering the bilinear coupling of polarization and OP gradients. The relation between the layer group approach and the Landau-Ginzburg free energy description is discussed, and two mechanisms of polarization switching inside the APBs are distinguished. It is illustrated that the polar APBs observed in PbZrO_3 are consistently and naturally explained by the layer group approach. This analysis is expected to have a significant impact also in other materials.

DOI: [10.1103/PhysRevB.104.224107](https://doi.org/10.1103/PhysRevB.104.224107)

I. INTRODUCTION

The perovskite oxide PbZrO_3 is usually considered the prototypic antiferroelectric (AFE) material. Its bulk and surface properties have been studied in detail by *ab initio* calculations [1–6], but to the best of our knowledge, domain wall (DW) properties have not been treated by atomistic simulations. DWs in ferroic materials became recently of increasing interest due to the substantial improvement of experimental techniques allowing their observation [7–10] and unveiling their potential for applications [11–13]. The tensor properties of DWs and, in particular, of antiphase boundaries (APBs) in perovskites were studied by several authors [10,14–18]. The occurrence of polarization inside the DWs in otherwise nonpolar samples was predicted based on symmetry analysis using the layer-group method [19,20] and also described by the phenomenological Landau-Ginzburg approach [18,21–25]. In the latter case, it is explained by flexoelectricity occurring at the center of the DWs due to the coupling of polarization and the strain gradient [16,26,27]. It turned out that, in addition to flexoelectricity, the so-called *rotopolar* effect can also be responsible for polarization, which is driven by the coupling of polarization and a Lifshitz-like gradient term of the order parameter (OP) [17,23]. A general approach based on the combination of OP symmetry and layer-group analysis was suggested and demonstrated for the study of the properties of DWs in KSCN [28], SrTiO_3 (STO) [29], and PbZrO_3 (PZO) [30]. The observation and modeling of the mi-

croscopic polar structure of APBs in AFE PZO are presented in Refs. [18,31,32], and the appearance of polarization at the APB center was explained by a biquadratic coupling between OP and polarization [18].

In this paper, we present an analysis of the polar properties of the APBs in PZO, especially linking between microscopic and macroscopic properties, and a manifestation of the microscopic symmetry in the phenomenological Landau-Ginzburg description.

II. SYMMETRY AND DOMAIN STATES
IN LEAD ZIRCONATE

The AFE phase transition in lead zirconate at $T_c = 505$ K transforms the crystal from the cubic perovskite phase $Pm\bar{3}m$ ($Z = 1$) to the orthorhombic phase $Pbam$ ($Z = 8$), with an eightfold multiplication of the cubic unit cell [33,34].

The unit cell (Fig. 1) of the AFE $Pbam$ phase with lattice vectors \mathbf{a}_o , \mathbf{b}_o , and \mathbf{c}_o is related to the cubic phase with $\mathbf{a}_c = (a, 0, 0)$, $\mathbf{b}_c = (0, a, 0)$, and $\mathbf{c}_c = (0, 0, a)$ as $\mathbf{a}_o = \mathbf{a}_c - \mathbf{b}_c$, $\mathbf{b}_o = 2(\mathbf{a}_c + \mathbf{b}_c)$, and $\mathbf{c}_o = 2\mathbf{c}_c$, with the origin shifted to $(\frac{a}{2}, 0, \frac{a}{2})$. This unit cell corresponds to the orthorhombic domain states (DSs) 1_i described below. Other orientational domains are obtained by appropriate rotations.

The soft mode behavior [2,27,36] is rather complicated and involves many modes. However, the space-group symmetry change can be well understood [37,38] as a result of the condensation of two OPs. The lead displacements are described by the condensation of a wave with a propagation vector $\mathbf{k}_\Sigma = \frac{2\pi}{a}(\frac{1}{4}, \frac{1}{4}, 0)$, with the following 12-component

^{*}rychet@fzu.cz

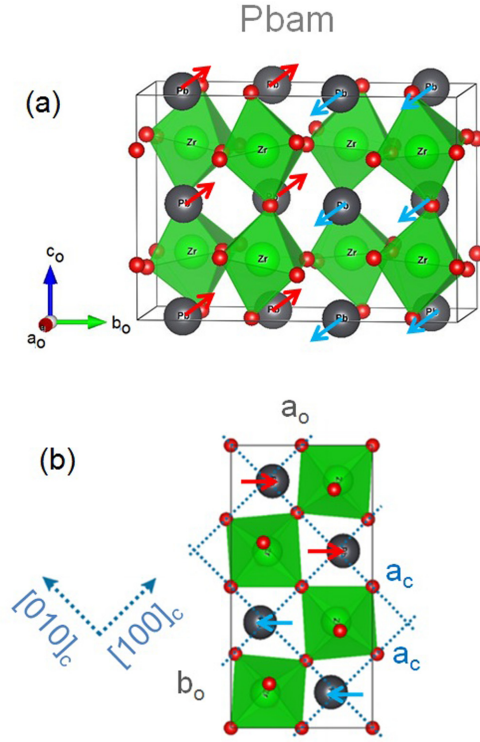


FIG. 1. Structure of PbZrO_3 [35]. (a) Crystal structure of the $Pbam$ unit cell of PbZrO_3 . (b) Projection of the $Pbam$ structure onto the (x, y) plane. The arrows indicate the displacements of the Pb cations in the Σ_2 mode. These Pb displacements along the pseudocubic $[1\bar{1}0]$ direction can be written [18] as $\mathbf{r}_{\text{Pb}} \propto (1, -1, 0)\cos[\frac{\pi}{2a_c}(x_c + y_c) + \varphi]$.

eigenvector:

$$\boldsymbol{\eta} = \{\eta_1, \eta_2, \eta_3, \eta_4, \eta_5, \eta_6, \eta_7, \eta_8, \eta_9, \eta_{10}, \eta_{11}, \eta_{12}\}, \quad (1)$$

which transforms according to the irreducible representation [39] Σ_2 . There are six orientational DSs, each described by one pair of OP components, as shown in Table I. Since the condensation of Σ_2 is associated with a fourfold increase in the number of atoms in the unit cell, every orientational DS can exist in four different translational DSs with respect to lead displacements [40], numbered by i -index in Table I, $i = 1, \dots, 4$. The equilibrium values of the OP pair (η_1, η_2) are $(\eta, -\eta)$, $(-\eta, -\eta)$, $(-\eta, \eta)$, and (η, η) for DSs

TABLE I. Symmetry-allowed OP components η_i in the six orientational DSs and corresponding octahedral tilts ϕ_i .

DSs	$\boldsymbol{\eta}$											$\boldsymbol{\phi}$					
1_i	η_1	η_2	0	0	0	0	0	0	0	0	0	0	0	0	0	0	0
2_i	0	0	η_3	η_4	0	0	0	0	0	0	0	0	0	0	ϕ_1	ϕ_2	0
3_i	0	0	0	0	η_5	η_6	0	0	0	0	0	0	0	0	0	ϕ_2	ϕ_3
4_i	0	0	0	0	0	0	η_7	η_8	0	0	0	0	0	0	0	0	0
5_i	0	0	0	0	0	0	0	0	η_9	η_{10}	0	0	0	ϕ_1	0	ϕ_3	0
6_i	0	0	0	0	0	0	0	0	0	0	0	η_{11}	η_{12}	0	0	0	0

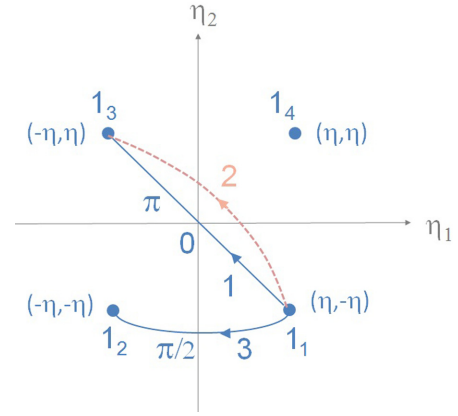


FIG. 2. Translational domain states (DSs) and antiphase boundaries (APBs) in order parameter (OP) space. Mapping of the translational DSs and APBs within a single orientational DS of PbZrO_3 in the subspace (η_1, η_2) of the OP space $\boldsymbol{\eta}$. Circles represent the four different DSs $1_1, 1_2, 1_3,$ and 1_4 , and lines describe some possible pathways of the corresponding APB in the OP space, e.g., line 1 represents an Ising wall between 1_1 and 1_3 , and line 2 is an improper Néel wall of the corresponding domain pair.

$1_1, 1_2, 1_3,$ and 1_4 , respectively. It is analogous for the remaining DSs.

The translational DSs within a given orientational state can be transformed from one to another by shifting the lattice by lost translations, e.g., DSs 1_i are related by $(a, 0, 0)$, $(2a, 0, 0)$, or $(3a, 0, 0)$, which after application of the matrix element $(1|t_1, t_2, t_3)$, $(t_1 = na, t_2 = ma, t_3 = la)$ of the irrep Σ_2 leads to the following identification:

$$\begin{aligned} 1_1 - \left(\mathbf{a}_c, \frac{\pi}{2}\right) &\rightarrow 1_2, \\ 1_1 - (2\mathbf{a}_c, \pi) &\rightarrow 1_3, \\ 1_1 - \left(3\mathbf{a}_c, \frac{3\pi}{2}\right) &\rightarrow 1_4, \end{aligned} \quad (2)$$

where it is shown that the corresponding lead displacement modes in different translational DSs are phase-shifted by $\Delta\varphi = \pi/2, \pi$ and $3\pi/2$, respectively (Fig. 2). The orientational DSs are related by rotations, DSs 1 and 2 by $\pi/2$ rotation about \mathbf{c}_c , 3 and 4 about \mathbf{a}_c , and 5 and 6 about \mathbf{b}_c . The AFE lead displacements are along cubic $(1, -1, 0)$ in 1_i and $(1, 1, 0)$ in 2_i DSs, $(1, 0, -1)$ in 3_i and $(1, 0, 1)$ in 4_i DSs, and $(0, 1, -1)$ in 5_i and $(0, 1, 1)$ in 6_i DSs.

A condensation of the Σ_2 mode alone would lead [38] to a $Pbam(4V)$ phase with a change of the unit cell volume by a factor of 4. To get the $Pbam(8V)$ phase, one has to consider the antiphase rotations of the oxygen octahedra, which are described by the condensation of a wave with $\mathbf{k}_R = \frac{2\pi}{a}(\frac{1}{2}, \frac{1}{2}, \frac{1}{2})$, with OP $\boldsymbol{\phi} = (\phi_1, \phi_2, \phi_3)$ transforming under the irrep R_4^+ and yielding a doubling of the unit cell in the c direction. Here, $\phi_1, \phi_2,$ and ϕ_3 represent octahedra rotations about $x, y,$ and z , respectively. The equilibrium OP for PbZrO_3 has always one 0 component, and it has two possible values, e.g., for DSs 1_i and 2_i , $(\phi_1, \phi_2, 0) = (\phi, -\phi, 0)$ or $(-\phi, \phi, 0)$, see Table I.

The symmetry breaking $Pm\bar{3}m(V) \rightarrow Pbam(8V)$ leads to $\frac{48}{8} \times 8 = 48$ DSs. Further, the symmetry of the $\pi/2$ and π

APBs is studied to find out the polar properties of the APBs and compare them with recent experimental results and simulations [18,31]. We use the approach based on the layer group analysis and Landau theory as it was suggested in previous papers.

III. SYMMETRIES OF OBJECTS RELATED TO DWs

The symmetry of the DW is closely related to other mathematical objects such as DSs, domain pairs (DPs), domain twins, etc., and for further calculations, it is convenient to introduce the following sequence of objects built from DSs A and B with lowering symmetry: Symmetry of unordered DP \supset symmetry of oriented DP \supset union of symmetries of DWs at all positions \supset symmetry of a single DW at position p . It can be formally written as

$$\begin{aligned} (A, B) + (B, A) &\supset (A, B)(\mathbf{n}) + (B, A)(-\mathbf{n}) \\ &\supset \sum_{p'} [(A, B)(\mathbf{n}) + (B, A)(-\mathbf{n})](\mathbf{p}') \\ &\supset [(A, B)(\mathbf{n}) + (B, A)(-\mathbf{n})](\mathbf{p}), \end{aligned} \quad (3)$$

and in short notation

$$\begin{aligned} S_0 &\equiv \{A, B\} \supset S_1 \equiv (A|\mathbf{n}|B) \supset S_2 \\ &\equiv \sum_{p'} (A|\mathbf{n}, \mathbf{p}'|B) \supset S_3 \equiv (A|\mathbf{n}, \mathbf{p}|B). \end{aligned} \quad (4)$$

The symmetries S_1 , S_2 , S_3 are used in the next sections. Note that the above description is related to the DW of two DSs A and B separated by a plane with the normal vector \mathbf{n} and position \mathbf{p} . Since such a wall contains only two domains, we refer to it as a simple DW.

In more complex DWs, a precursor (nucleus) of an additional DS, say C , may occur at the DW center [22,23]. The symmetry operations of C yield further restrictions on symmetry, and it is encountered in the expression in Eq. (3) as

$$\begin{aligned} [(A, B) + (B, A)](C) &\supset [(A, B)(\mathbf{n}) + (B, A)(-\mathbf{n})](C) \\ &\supset \left\{ \sum_{p'} [(A, B)(\mathbf{n}) + (B, A)(-\mathbf{n})](\mathbf{p}') \right\} (C) \\ &\supset [(A, B)(\mathbf{n}) + (B, A)(-\mathbf{n})](C)(\mathbf{p}). \end{aligned} \quad (5)$$

Note that the last expression in Eq. (5) in principle describes the DW between A and B separated by the plane with normal \mathbf{n} and position \mathbf{p} and with C at the center. Its short notation can be $(A|C, \mathbf{n}, \mathbf{p}|B)$ [compare with Eq. (4)]. It should be stressed that we always consider a single DW with one plane \mathbf{n} and one position \mathbf{p} . For comparison, note that one can also study a structure of two separated DWs: $(A|\mathbf{n}_1, \mathbf{p}_1|C) + (C|\mathbf{n}_2, \mathbf{p}_2|B)$. Here, C denotes a fully developed DS, while C above means a nucleus of C at the center. In the next sections, it will also be shown that the symmetry S_2 is reflected in the free energy gradient invariants, while the microscopic positions of DWs inside the unit cell are invisible by the Landau-Ginzburg approach.

To avoid misunderstanding, we further use the following naming of the APBs. The APB $(A|B)$ composed of two translational DSs is mentioned as Ising-like. The APB $(A|C|B)$

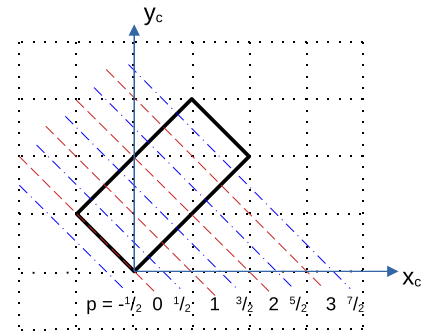


FIG. 3. Unit cell of the 1_1 domain state (DS) and potentially significant positions of the antiphase boundary (APB). The position p is determined by the intersection of the APB plane (color lines) with the x axis. The set of blue domain walls (DWs; if any) possess the same point symmetry, and the same applies to the set of red DWs (examples are in Secs. IV and V). The cubic coordinates are used.

with nucleus (precursor) of the translational DS C with respect to A and B is called improper Néel-like (see the path 2 in Fig. 2). If C represents a different orientational DS, then $(A|C|B)$ is called a (proper) Néel structure.

IV. ON THE POLARIZATION IN $(1_1|1_2)$ APB

Let us consider the $\pi/2$ -type APB between the DSs 1_1 and 1_2 (Fig. 2), which were defined in the previous section. Here, $1_1 = (\eta, -\eta, 0, \dots, 0)$ and $1_2 = (-\eta, -\eta, 0, \dots, 0)$, both with octahedra rotations $(\phi, -\phi, 0)$, see Table I. The normal of the DW plane \mathbf{n} can be taken arbitrarily; here, we consider $\mathbf{n} = (1, 1, 0)$ since it was recently discussed by several authors. The microscopic position of the APB inside the unit cell is denoted as \mathbf{p} , and for the moment, it is left arbitrary. All possible positions and corresponding symmetries will be generated during the calculation, Fig 3. The APB between DSs 1_1 and 1_2 , with the normal \mathbf{n} and position \mathbf{p} is denoted as $(1_1|\mathbf{n}, \mathbf{p}|1_2)$. For further analysis, we consider the symmetries of the following three objects (see (4)):

(i) The symmetry S_1 of the object $(1_1|\mathbf{n}|1_2)$ [note that $(1_1|\mathbf{n}|1_2) \equiv (1_2|-\mathbf{n}|1_1)$] consists of all operations which either leave the DSs and the normal invariant or interchange DSs and, at the same time, reverse the normal vector. All operations from S_1 keep the orientation of the DW plane fixed, but some of them can move the plane along the normal \mathbf{n} .

(ii) Symmetry S_2 of object $(1_1|\mathbf{n}, \mathbf{p}_{\text{arb}}|1_2)$, where the arbitrary position \mathbf{p}_{arb} of the APB is considered (all possible positions are considered). Here, S_2 is obtained from S_1 by choosing only operations which do not move the DW plane along \mathbf{n} . The position of the DW is defined as the point where the plane intersects the x axis, $\mathbf{p} = (p, 0, 0)$, see Fig. 3. The point (x, y, z) lies in the plane positioned at $\mathbf{p} = (p, 0, 0)$, when $\mathbf{n} \cdot (x, y, z) = \mathbf{n} \cdot \mathbf{p}$. In our case, it yields $x + y = p$. The transformed point (x', y', z') lies in the same plane if $\mathbf{n} \cdot (x', y', z') = \mathbf{n} \cdot \mathbf{p}$, i.e., $x' + y' = p$. We can apply these equations to the elements of S_1 [see (iii) below] and obtain the positions p , e.g., for the first operation, the equation of the plane reads $(-x + 1) + (-y + 1) = p$, and since $x + y = p$, it yields the position $p = 1$. The positions of planes invariant with respect to individual operations are listed in Eq. (6)

just behind S_1 . Here, $p = p$ means that any position is possible, while $p = -$ indicates no solution, i.e., the last two operations shift the plane along \mathbf{n} . Now it is clear that S_2 corresponds to the union of symmetry operations of APBs at all positions. In this way, we automatically obtained all possible positions of the APBs, two special positions $p = 0, 1$ (high symmetric) and a general position p (low symmetric, neither 0 nor 1), see below. The average symmetry S_2 determines whether a macroscopic polarization can exist. Since its point group contains the inversion element, the macroscopic polarization does not exist, and therefore, there are no Landau free energy expansion terms which could generate it (see the next section).

(iii) The microscopic symmetries S_3 (*the layer groups*) of the APB $(1_1|\mathbf{n}, \mathbf{p}|1_2)$ at particular microscopic positions p are obtained from S_2 by extracting the operations with particular values of p :

$$S_1 = \begin{pmatrix} \bar{x} + 1 & \bar{y} + 1 & \bar{z} \\ \bar{x} + 1 & \bar{y} + 1 & z + 1 \\ x & y & \bar{z} + 1 \\ x & y & z \\ \bar{y} & \bar{x} & \bar{z} \\ \bar{y} & \bar{x} & z + 1 \\ y + 1 & x + 1 & \bar{z} + 1 \\ y + 1 & x + 1 & z \end{pmatrix} p = \begin{pmatrix} 1 \\ 1 \\ p \\ p \\ 0 \\ 0 \\ - \\ - \end{pmatrix},$$

$$S_2 = \begin{pmatrix} \bar{x} + 1 & \bar{y} + 1 & \bar{z} \\ \bar{x} + 1 & \bar{y} + 1 & z + 1 \\ x & y & \bar{z} + 1 \\ x & y & z \\ \bar{y} & \bar{x} & \bar{z} \\ \bar{y} & \bar{x} & z + 1 \end{pmatrix} p = \begin{pmatrix} 1 \\ 1 \\ p \\ p \\ 0 \\ 0 \end{pmatrix}. \quad (6)$$

$$S_3(p = 0) = \begin{pmatrix} \bar{y} & \bar{x} & \bar{z} \\ \bar{y} & \bar{x} & z + 1 \\ x & y & \bar{z} + 1 \\ x & y & z \end{pmatrix},$$

$$S_3(p = 1) = \begin{pmatrix} \bar{x} + 1 & \bar{y} + 1 & \bar{z} \\ \bar{x} + 1 & \bar{y} + 1 & z + 1 \\ x & y & \bar{z} + 1 \\ x & y & z \end{pmatrix}, \quad (7)$$

$$S_3(p = \text{gen}) = \begin{pmatrix} x & y & \bar{z} + 1 \\ x & y & z \end{pmatrix}.$$

Here, $S_3(p = 0)$ allows $\mathbf{P} = (P, -P, 0)$; $S_3(p = 1)$ is nonpolar; S_2 is average symmetry (we can call it *macroscopic*), and

it is nonpolar, in agreement with invariants, as will be shown below.

Allowed translations corresponding to $S_1, S_2,$ and S_3 are

$$\mathbf{T}_1 = [k(0, 0, 2), l(1, -1, 0), m(2, 2, 0)],$$

$$\mathbf{T}_2 = \mathbf{T}_3 = [k(0, 0, 2), l(1, -1, 0)].$$

Let us note that, in general, there are symmetrically equivalent APBs at positions $p = \dots, -3, -1, +1, +3, \dots$, and another set of APBs at $p = \dots, -2, 0, +2, \dots$. The symmetry operation $\bar{x} + 1, \bar{y} + 1, z + 1$ of APB($p = 1$) transforms the APB($p = 0$) with $+\mathbf{P}$ to the APB($p = 2$) with reversed polarization $-\mathbf{P}$. The last two operations in the matrix S_1 have a similar effect. The graphical representation of the Ising-like APB $(1_1|1_2)$ at the possible positions discussed before is shown in Fig. 4. The polarization at the center is reversed when shifting the APB from $p = 0$ to 2. The polarization profiles at these positions have the form of a single peak, while the profile at $p = 1$ has an antisymmetric shape. The polarization averaged over all positions is zero, as predicted by S_2 . Let us mention in advance that the symmetry S_2 also indicates that the macroscopic polarization profile obtained from the free energy description is exactly zero, see curve 1 in Fig. 8.

To get a macroscopic polarization, an additional symmetry lowering of $(1_1|\mathbf{n}|1_2)$ is needed. It can be achieved in the APB of the Néel type with a nucleus of another DS at the center, which can occur due to a local phase transition in the DW [22,23,41]. We consider $(1_1|2_1, \mathbf{n}, \mathbf{p}|1_2)$, i.e., there is in addition the nucleus 2_1 (orientational DS) at the APB center, see Sec. III and comments therein. The procedure outlined above yields

$$S_1 = S_2 = S_3(p = 0) = \begin{pmatrix} x & y & \bar{z} + 1 \\ x & y & z \\ \bar{y} - 1 & \bar{x} + 1 & \bar{z} \\ \bar{y} - 1 & \bar{x} + 1 & z + 1 \end{pmatrix} p = \begin{pmatrix} p \\ p \\ 0 \\ 0 \end{pmatrix}, \quad (8)$$

and $S_3(p = \text{gen})$ is the same as in Eq. (7). In this case, the APB is (macroscopically) polar, $\mathbf{P} = (P, -P, 0)$, and note that there is only one set of positions of the APB with high symmetry, $p = \dots, -2, 0, 2, \dots$. The APBs at $p = 0$ and 2 have the same symmetry-allowing polarization $(P, -P, 0)$, but they are not related by any operation, and therefore, their polarization vectors cannot cancel.

Allowed translations corresponding to $S_1, S_2,$ and S_3 are

$$\mathbf{T}_1 = [k(0, 0, 2), l(2, -2, 0), m(2, 2, 0)],$$

$$\mathbf{T}_2 = \mathbf{T}_3 = [k(0, 0, 2), l(2, -2, 0)].$$

To be more precise and avoid misunderstanding concerning Eq. (8), let us note that the full symmetries are related as

$$(S_1 \oplus \mathbf{T}_1) \supset (S_2 \oplus \mathbf{T}_2) \\ = [S_3(p = 0) \oplus \mathbf{T}_3] \supset [S_3(p = \text{gen}) \oplus \mathbf{T}_3].$$

The Néel-like APB $(1_1|2_1|1_2)$ with the nucleus 2_1 is illustrated in Fig. 5. Note that the polarizations at positions

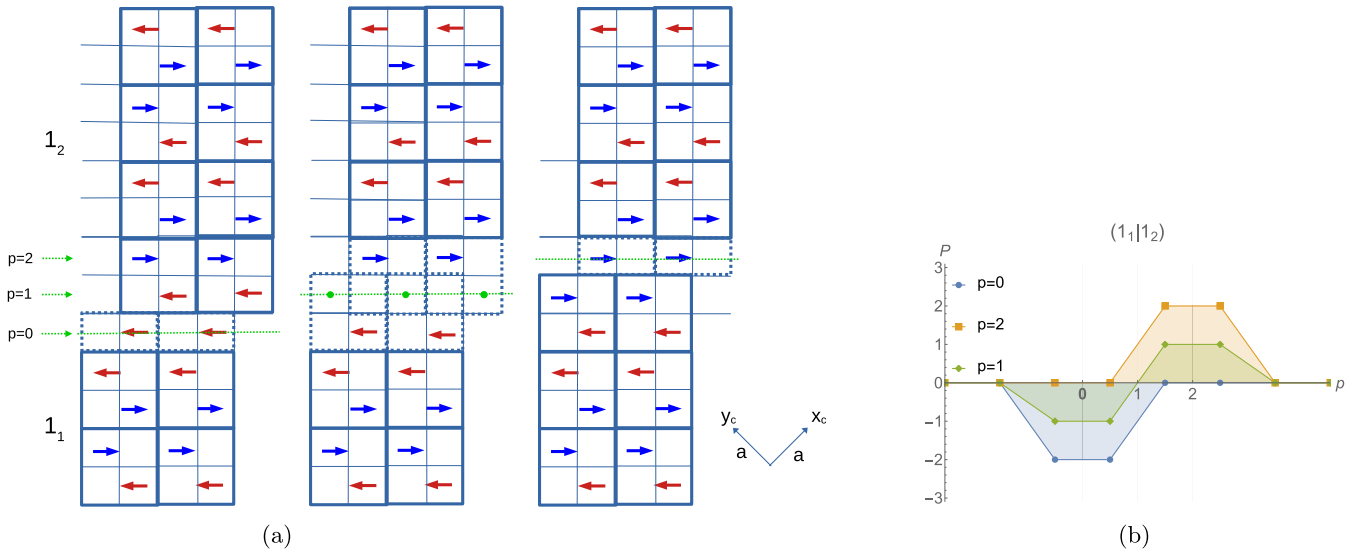


FIG. 4. $\pi/2$ antiphase boundary (APB) $(1_1|1_2)$ (Ising-like type) at different positions. (a) The APBs at $p = 0$ and 2 are symmetry related and have opposite polarizations. The APB at $p = 1$ has higher symmetry with an antisymmetric polarization profile. (b) The polarization profiles of the APBs were obtained by the sliding unit cell method. The macroscopic polarization is an average over all positions and yields 0.

$p = 0$ and 2 have again opposite signs, but the mean value is nonzero. It means a nonzero macroscopic polarization, qualitatively shown in curve 3 of Fig. 8.

V. SYMMETRY OF $(1_1|1_3)$ APB

Here, the procedure outlined in the previous section is used to study the symmetry and polarity of the APBs

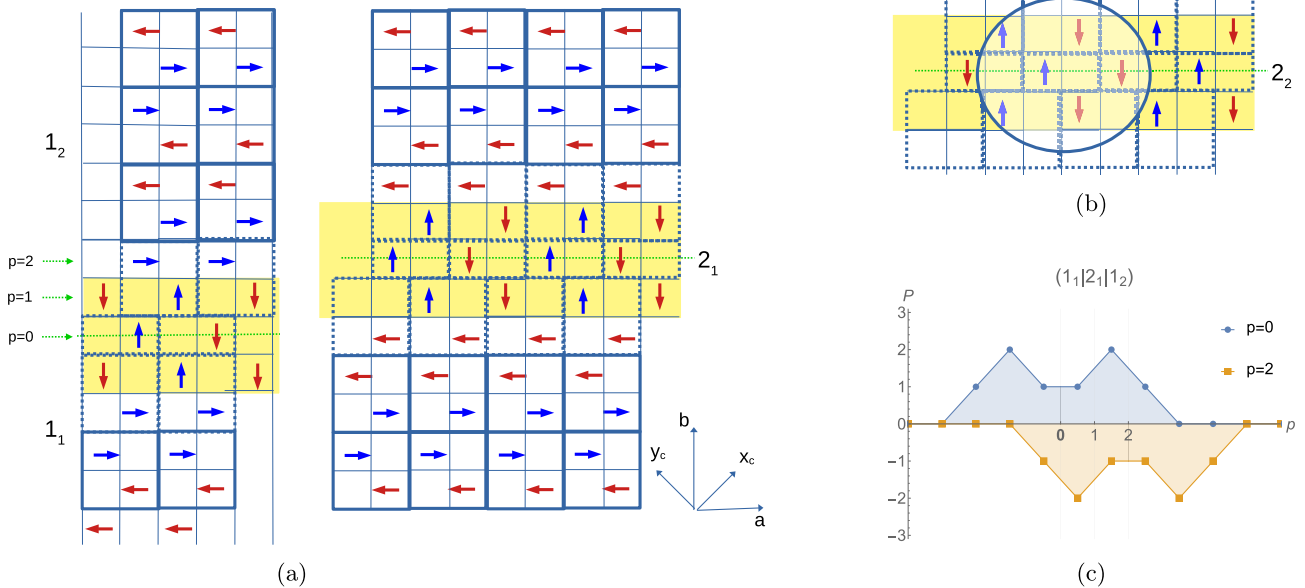


FIG. 5. $\pi/2$ antiphase boundary (APB) with a nucleus: $(1_1|2_1|1_2)$ (Néel-like type). (a) There are only two high-symmetric positions $p = 0, 2$ (see dotted green lines) as compared with Fig. 4, and they are not related by any symmetry operation. The nucleus 2_1 shows the left-oriented wedge pattern. (b) The nucleus 2_2 with the right-oriented wedge pattern. The switching from 2_1 to 2_2 in (a) is accomplished by the reversal of arrows in the central row. (c) The sliding unit cell calculation of the polarization profiles of $(1_1|2_1|1_2)$. The double peak reflects the presence of two interfaces $1_1|2_1$ and $2_1|1_2$ at the center of the wall. The polarizations at $p = 0$ and 2 are still opposite and seemingly equal, as in Fig. 4, but in reality, they differ since symmetry S_2 dictates a nonzero average of in-plane polarization P .

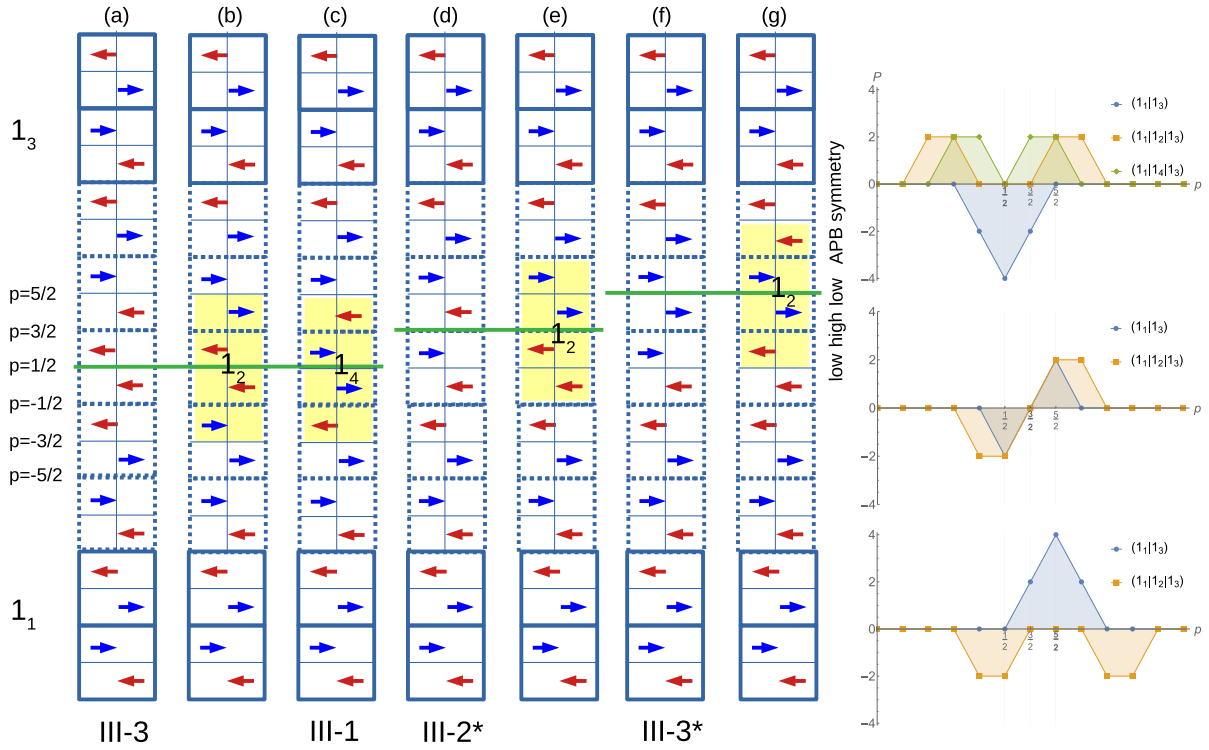


FIG. 6. Selected π antiphase boundaries (APBs). Left: The green lines show the positions of the APBs. The APBs discussed in Refs. [18,31] are indicated by the symbols at the bottom. The symbol * denotes symmetrically equivalent APBs at different positions than in Ref. [18,31], e.g., III-2 is at $p = -\frac{1}{2}$, while III-2* is at $p = \frac{3}{2}$. Right: The polarization profiles of the APBs were obtained by the sliding unit cell method. The double peak is caused by a nucleus at the center of the APB.

between 1_1 and 1_3 DSs with Ising-like and Néel-like structures (Fig. 2). The symmetries related to the Ising-like ($1_1|1_3$) APB read

$$S_1 = \begin{pmatrix} \bar{x} + 1 & \bar{y} + 2 & \bar{z} + 1 \\ \bar{x} + 1 & \bar{y} + 2 & z \\ x & y & \bar{z} + 1 \\ x & y & z \\ \bar{y} + 1 & \bar{x} & \bar{z} + 1 \\ \bar{y} + 1 & \bar{x} & z \\ y + 1 & x + 1 & \bar{z} + 1 \\ y + 1 & x + 1 & z \end{pmatrix} p = \begin{pmatrix} \frac{3}{2} \\ \frac{3}{2} \\ p \\ p \\ \frac{1}{2} \\ \frac{1}{2} \\ - \\ - \end{pmatrix}, \quad (9)$$

$$S_2 = \begin{pmatrix} \bar{x} + 1 & \bar{y} + 2 & \bar{z} + 1 \\ \bar{x} + 1 & \bar{y} + 2 & z \\ x & y & \bar{z} + 1 \\ x & y & z \\ \bar{y} + 1 & \bar{x} & \bar{z} + 1 \\ \bar{y} + 1 & \bar{x} & z \end{pmatrix} p = \begin{pmatrix} \frac{3}{2} \\ \frac{3}{2} \\ p \\ p \\ \frac{1}{2} \\ \frac{1}{2} \end{pmatrix}.$$

$$S_3 \left(p = \frac{1}{2} \right) = \begin{pmatrix} \bar{y} + 1 & \bar{x} & \bar{z} + 1 \\ \bar{y} + 1 & \bar{x} & z \\ x & y & \bar{z} + 1 \\ x & y & z \end{pmatrix},$$

$$S_3 \left(p = \frac{3}{2} \right) = \begin{pmatrix} \bar{x} + 1 & \bar{y} + 2 & \bar{z} + 1 \\ \bar{x} + 1 & \bar{y} + 2 & z \\ x & y & \bar{z} + 1 \\ x & y & z \end{pmatrix}. \quad (10)$$

$$S_3(p = \text{gen}) = \begin{pmatrix} x & y & \bar{z} + 1 \\ x & y & z \end{pmatrix},$$

$$\mathbf{T}_1 = [k(0, 0, 2), l(1, -1, 0), m(2, 2, 0)],$$

$$\mathbf{T}_2 = \mathbf{T}_3 = [k(0, 0, 2), l(1, -1, 0)].$$

The APBs at positions $p = \dots, -\frac{3}{2}, \frac{1}{2}, \frac{5}{2}, \dots$ have the same symmetry and allow the polarization along $(1, -1, 0)$ but with alternating sign, e.g., if the APB($p = \frac{1}{2}$) has polarization $(P, -P, 0)$, then the APB($p = \frac{5}{2}$), which is obtained from APB($p = \frac{1}{2}$) using either of the two last operations in S_1 , e.g., $(y + 1, x + 1, z)$ [or using $(\bar{x} + 1, \bar{y} + 1, z)$ from S_2] possesses polarization $(-P, P, 0)$. All the APBs at $p = \dots, -\frac{1}{2}, \frac{3}{2}, \frac{7}{2}, \dots$ are nonpolar (antisymmetric profiles).

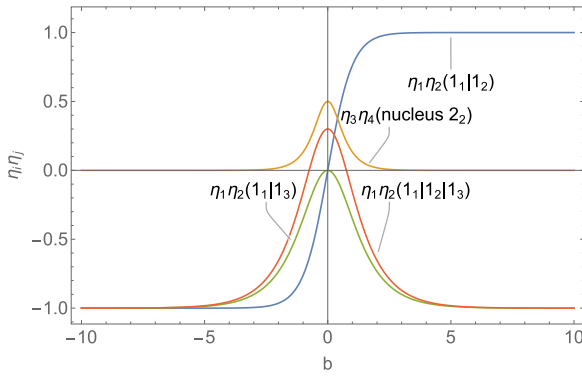


FIG. 7. The schematic $\eta_1\eta_2$ profiles of the antiphase boundary (APB). In the APBs with the nucleus 2_2 , the profiles consist of two curves: $\eta_1\eta_2$ and $\eta_3\eta_4$. All curves are either even or odd functions.

The corresponding Ising-like APBs at the three significant positions are depicted as (a), (d), and (f) in Fig. 6 together with their microscopic polarization profiles. The macroscopic polarization profile determined by the S_2 symmetry is identically zero, as shown by curve 1 in Fig. 8.

A. Symmetry of $(1_1|1_2|1_3) = \text{symmetry of } (1_1|1_3)$

Interestingly enough, it turns out that the symmetry properties of the improper Néel-type APB $(1_1|1_2|1_3)$ are identical with the Ising-like $(1_1|1_3)$. Its structures at three symmetric positions are illustrated as pictures (b), (e), (g) in Fig. 6. Note that the polarization profiles reveal a double peak due to the two interphases $1_1|1_2$ and $1_2|1_3$ nearby the center of the APB. The macroscopic polarization profile is, as in the previous case $(1_1|1_3)$, identically zero.

B. Symmetry of $(1_1|2_2|1_3)$

The appearance of the orientational/translational nucleus 2_2 at the center of $(1_1|1_3)$, with the Pb displacements along $(1, 1, 0)$, results in the symmetry lowering; the only high-symmetry positions $p = \dots, -\frac{1}{2}, \frac{3}{2}, \frac{7}{2}, \dots$ correspond to the

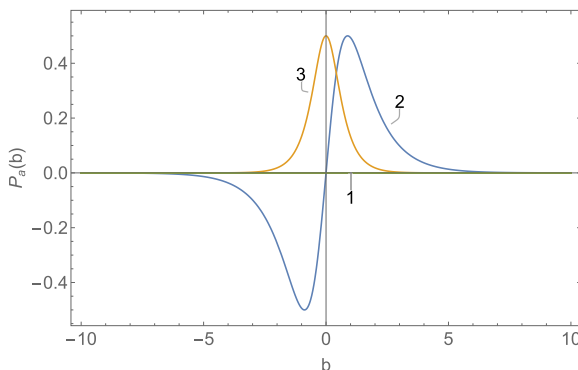


FIG. 8. The schematic polarization $P_a(b)$ profiles. 1: Antiphase boundaries (APBs) $(1_1|1_2)$, $(1_1|1_3)$, and $(1_1|1_2|1_3)$; 2: APB $(1_1|2_2|1_3)$; and 3: APB $(1_1|2_2|1_2)$.

nonpolar APBs, compare with Eqs. (9) and (10):

$$S_1 = S_2 = S_3 \left(p = \frac{3}{2} \right) = \begin{pmatrix} \bar{x} + 1 & \bar{y} + 2 & \bar{z} + 1 \\ \bar{x} + 1 & \bar{y} + 2 & z \\ x & y & \bar{z} + 1 \\ x & y & z \end{pmatrix}$$

$$p = \begin{pmatrix} \frac{3}{2} \\ \frac{3}{2} \\ p \\ p \end{pmatrix}, \quad (11)$$

$$S_3(p = \text{gen}) = \begin{pmatrix} x & y & \bar{z} + 1 \\ x & y & z \end{pmatrix}, \quad (12)$$

$$\mathbf{T}_1 = [k(0, 0, 2), l(2, -2, 0), m(2, 2, 0)],$$

$$\mathbf{T}_2 = \mathbf{T}_3 = [k(0, 0, 2), l(2, -2, 0)].$$

Note that there is only one high-symmetry position at $p = \frac{3}{2}$. We do not plot the structure of this APB explicitly, but one can find that the microscopic sliding-cell profile is antisymmetric [it is qualitatively like the profile of $(1_1|1_3)$ at $p = \frac{3}{2}$ in Fig. 6]. It is interesting that, in this case, the symmetry S_2 allows the macroscopic polarization profile, which is antisymmetric, see curve 2 in Fig. 8, Sec. VI.

C. Symmetry of $(1_1|3_2|1_3)$

Note that the Pb displacements in all DSs 1_1 , 1_2 , 1_3 , and 2_2 considered so far in the APBs lie in the xy plane. Unlike the previous walls, the nucleus 3_2 has the Pb displacements lying in the yz plane, inclined $\pi/4$ rad from the xy plane. The symmetries are

$$S_1 = S_2 = S_3 \left(p = \frac{3}{2} \right) = \begin{pmatrix} \bar{x} + 2 & \bar{y} + 1 & \bar{z} + 1 \\ x & y & z \end{pmatrix}$$

$$p = \begin{pmatrix} \frac{3}{2} \\ p \end{pmatrix}, \quad (13)$$

$$S_3(p = \text{gen}) = \begin{pmatrix} x & y & \bar{z} + 1 \\ x & y & z \end{pmatrix}, \quad (14)$$

$$\mathbf{T}_1 = [k(2, -2, 2), l(-2, 2, 2), m(2, 2, -2)],$$

$$\mathbf{T}_2 = \mathbf{T}_3 = [k(2, -2, 2), l(-2, 2, 2)].$$

The high-symmetric positions $p = \dots, -\frac{1}{2}, \frac{3}{2}, \frac{7}{2}, \dots$ correspond again to the nonpolar APBs.

VI. FREE ENERGY INVARIANTS AND PROFILES

The macroscopic properties of DWs can be described by the Landau-Ginzburg free energy, and it is interesting to compare it with the layer-group approach discussed in the previous section. The polarization in the DWs is described by the free energy invariants, which couple the polarization and OP as well as gradient terms. In general, there is a large number of invariants, and they are shown in Appendix.

Tagantsev *et al.* [18] proposed a biquadratic coupling of polarization and OP to explain the polarization in APBs. However, it is clear that the biquadratic coupling terms alone cannot explain the wealth of observed polarization profiles. Here, we focus on bilinear couplings of polarization and gradients of OP. The biquadratic and bilinear cases will be compared in terms of their implications to explain the observations. The APBs in the previous sections have the DW normal $\mathbf{n} \perp z$ and the only nonzero OP components η_1, \dots, η_6 . Therefore, it is enough to assume $\partial_z(\cdot) = 0$ and $\eta_7 = \dots = \eta_{12} = 0$. If we further consider only 1 and 2 orientational states, then also $\eta_5 = \eta_6 = 0$ and the number of nonzero invariants reduces to 12. Only the following two of them give the in-plane polarization $\mathbf{P} \perp \mathbf{n} = 0$:

$$\begin{aligned} U_{L5} &= (P_x \partial_x - P_y \partial_y)(\eta_1 \eta_2 \eta_3 \eta_4) \\ &= (P_a \partial_b + P_b \partial_a)(\eta_1 \eta_2 \eta_3 \eta_4) = P_a \partial_b (\eta_1 \eta_2 \eta_3 \eta_4), \end{aligned} \quad (15)$$

$$\begin{aligned} V_{T1} &= \eta_3 \eta_4 (P_y \partial_x - P_x \partial_y)(\eta_1 \eta_2) + \eta_1 \eta_2 (P_x \partial_y - P_y \partial_x)(\eta_3 \eta_4) \\ &= \eta_1 \eta_2 (P_a \partial_b - P_b \partial_a)(\eta_3 \eta_4) - \eta_3 \eta_4 (P_a \partial_b - P_b \partial_a)(\eta_1 \eta_2) \\ &= P_a [\eta_1 \eta_2 \partial_b (\eta_3 \eta_4) - \eta_3 \eta_4 \partial_b (\eta_1 \eta_2)], \end{aligned} \quad (16)$$

where the orthorhombic axis b is along $\mathbf{n} = (1, 1, 0)$, a is along $(1, -1, 0)$, and $b = \frac{1}{\sqrt{2}}(x + y)$, and $a = \frac{1}{\sqrt{2}}(x - y)$, see also insets in Figs. 4 and 5. The simplest profiles of quadratic terms $\eta_i \eta_j$ satisfying the boundary conditions of individual APBs are sketched in Fig. 7. The polarization profiles of APBs can be obtained from the invariants in Eqs. (15) and (16), considering that the quadratic forms $\eta_i \eta_j$ are either odd or even functions as shown in Fig. 7, e.g., $\eta_1 \eta_2$ is an odd profile in $(1_1|1_2)$ APB, while it is an even function in $(1_1|1_3)$ APB.

Their properties also follow from the symmetries S_2 . Using the symmetry operations S_2 in Eqs. (6) and (9), the profiles of the APBs $(1_1|1_2)$, $(1_1|1_3)$, and $(1_1|1_2|1_3)$ satisfy $P_a(b) = -P_a(-b) = P_a(-b) \equiv 0$, in agreement with curve 1 in Fig. 8. The polarization profile of $(1_1|2_2|1_3)$ according to S_2 in Eq. (11) is asymmetric (odd): $P_a(b) = -P_a(-b)$, as shown in curve 2. Finally, based on S_2 in Eq. (8), the APB $(1_1|2_2|1_2)$ has symmetrical (even) profile since $P_a(b) = P_a(-b)$ (see curve 3), i.e., the only case with macroscopic in-plane polarization.

VII. DISCUSSION

The symmetry and properties of DWs on the microscopic level, i.e., in the sense that the position of the DW inside the unit cell is also important, can be well described by layer groups [19,28–30]. Here, this method was systematically applied to PZO by using the irreps of OPs to calculate the symmetries of the planar APBs. This method unveils that the microscopic polar properties of APBs depend on the APB type and their position. The APBs composed of the translational domains 1_i only, i.e., $(1_1|1_2)$, $(1_1|1_3)$, $(1_1|1_2|1_3)$, and $(1_1|1_4|1_3)$, possess three high-symmetry positions; two of them at $p = \frac{1}{2}$ and $\frac{5}{2}$ are polar with opposite polarizations, while the central position of higher symmetry in-between has an antisymmetric polarization profile, see Figs. 4 and 6. Several APBs of this kind were observed and analyzed by Wei *et al.* [18,31], and their properties can be understood using our approach, e.g., they measured and modeled the APB

denoted as III-1 (fig. 1 in Wei *et al.* [31]) and observed a double peak of polarization. We identify it as the improper Néel-type APB $(1_1|1_4|1_3)$ at $p = \frac{1}{2}$ with nonzero polarization of the double peak shape, Fig. 6. The double peak arises from two interfaces $1_1|1_4$ and $1_4|1_3$ near the boundary center. There exists, as mentioned above, an equivalent position of the APB $p = \frac{5}{2}$ with opposite polarization. In agreement with this, the observation of polar $(1_1|1_4|1_3)$ APB at two microscopic positions was reported [31]. For comparison, APBs I-1, I-2 in Ref. [31] are identified here as $(1_1|1_2)$ at two positions (Fig. 4), II-1 and II-2 are $(1_1|1_4)$ at two positions, and III-2 and III-3 are $(1_1|1_3)$ at two positions (Fig. 6). The polarization profiles at the right side of Figs. 4–6 were calculated using the method of sliding orthorhombic unit cell [18], but it should be treated only as an approximate visualization, e.g., the average in-plane polarization in the APB $(1_1|2_1|1_2)$ shown in Fig. 5 is not zero. The decisive element for the microscopic polar properties is the layer-group symmetry S_3 of each APB.

The DWs are also often described by Landau-Ginzburg theory. Here, we argue that such a coarse-grained theory cannot explain all features of the APBs because their properties depend on the microscopic position inside the unit cell, which cannot be fully accounted by the phenomenological approach. In previous Secs. III–V, we have demonstrated that the polarization (including its sign) in some APBs is obtained simply by appropriate choice of the APB position inside the unit cell. In general, the microscopic properties of APBs are properly described by the layer groups (S_3) only, but still there is a connection with the phenomenological description, which is determined by the average symmetry S_2 . For that, we use the following notation: \bar{P}_a is an average in-plane polarization, which is the same for both the layer group description and the phenomenological description, and $P_a(b)$ is a macroscopic (Landau-Ginzburg) polarization profile allowed by S_2 and described by Eqs. (15) and (16). Let us summarize the behavior of macroscopic in-plane polarization P_a determined by the symmetry S_2 for three instructive examples:

- (i) In purely translational APBs $(1_1|1_2)$, $(1_1|1_3)$, and $(1_1|1_2|1_3)$: $\bar{P}_a = 0$, $P_a(b) \equiv 0$.
- (ii) In the APB with two different orientational states $(1_1|2_1|1_3)$: $\bar{P}_a = 0$, $P_a(b) = -P_a(-b) \neq 0$.
- (iii) In the APB with two different orientational states $(1_1|2_1|1_2)$: $\bar{P}_a \neq 0$, $P_a(b) = P_a(-b) \neq 0$.

The corresponding macroscopic profiles are plotted in Fig. 8.

This entitles us to conclude that the macroscopic in-plane polarization (symmetric or antisymmetric profiles) can exist only in the APBs with a different orientational state at the center. It is in agreement with the macroscopic polarization P_a described by the free energy invariants in Eqs. (15) and (16); the latter is sometimes called rotopolar. For comparison, the biquadratic coupling $P_i^2 \eta_j^2$ proposed in Ref. [18] implies $\bar{P}_a \neq 0$ for the APB $(1_1|1_3)$, but it contradicts with point (i).

The polarization of the APBs observed in Ref. [31], which contain only translational DSs, cannot be described by the (continuous) Landau-Ginzburg theory but only by the layer-group approach. It is worth mentioning that one can distinguish two types of APBs with the nucleus (DS precursor) at the center (Sec. III). The first one is an improper Néel-type structure in the sense that the APB contains only translational

DSs [e.g., $(1_1|1_4|1_3)$ displayed as path 2 circumventing the origin in Fig. 2, in which all Pb displacements are parallel], and its symmetry is identical with $(1_1|1_3)$. The second one is a proper Néel-type structure with a different orientational state at the center [e.g., $(1_1|2_1|1_3)$], in which the symmetry is lowered compared with the APB $(1_1|1_3)$. Such a Néel structure can develop by means of the phase transition in the APB, and its properties (e.g., symmetric in-plane polarization) can be well described by the Landau-Ginzburg theory, which are fully in accord with the layer-group theory.

The symmetry properties of the APBs determine possibilities of the (in-plane) polarization reversal in both types of APBs by reversing the homogeneous electric field E_a applied along the a axis. Two cases can be distinguished. The reversal of the in-plane microscopic polarization in the macroscopically nonpolar APBs is accompanied with the shift of the APB position within the unit cell, e.g., the polarization $+P$ of the APB $(1_1|1_3)$ at $p = \frac{1}{2}$ is reversed to $-P$ via a shift to $p = \frac{5}{2}$ (or $-\frac{3}{2}$). The polarization switching in the macroscopically polar APBs is rendered by the transformation of the nucleus (DS precursor) at the center to a new DS, e.g., $+P$ in the APB $(1_1|2_1|1_2)$ is switched to $-P$ in the APB $(1_1|2_2|1_2)$, as can also be seen from Eq. (16). The switching mechanism is illustrated in Fig. 5.

The method used in this contribution for APBs in PZO is readily applicable for DWs in other materials.

ACKNOWLEDGMENTS

This paper was supported by Operational Program Research, Development and Education (financed by European Structural and Investment Funds and by the Czech Ministry of Education, Youth, and Sports), Project No. SOLID21-CZ.02.1.01/0.0/0.0/16_019/0000760.

APPENDIX: THE FREE ENERGY INVARIANTS

The occurrence of polarization in the DWs can be described by the free energy invariants with bilinear coupling of polarization and OP gradients. In general, there is a huge number of invariants, but it can be simplified considering DWs from previous sections with the DW normal $\mathbf{n} \perp z$ and the only nonzero OP components η_1, \dots, η_6 . Therefore, in the following text, we assume $\partial_z = 0$ and $\eta_7 = \dots = \eta_{12} = 0$. The are only three lowest order invariants with quadratic OP components:

$$T_1 = P_y \partial_x (\eta_1^2 + \eta_2^2 - \eta_3^2 - \eta_4^2) + P_x \partial_y (\eta_1^2 + \eta_2^2 - \eta_3^2 - \eta_4^2) + P_z \partial_x (\eta_5^2 + \eta_6^2), \quad (\text{A1})$$

$$T_2 = P_y \partial_y (\eta_5^2 + \eta_6^2), \quad (\text{A2})$$

$$T_3 = P_x \partial_x (\eta_1^2 + \eta_2^2 + \eta_3^2 + \eta_4^2 + \eta_5^2 + \eta_6^2) + P_y \partial_y (\eta_1^2 + \eta_2^2 + \eta_3^2 + \eta_4^2). \quad (\text{A3})$$

The next lowest invariants are those with quartic coupling of the OP components. There are in total 39 invariants, or 25 when using the above assumptions, see Tables II and III. Notations U , V , and W correspond to the columns in Table III; subscripts L and T denote longitudinal and transverse invari-

TABLE II. Total number of invariants. The invariant forms and their count are indicated, e.g., in the first column: number of invariants of type $P_m \partial_m (\eta_i \eta_j \eta_k \eta_l)$ is 15 (longitudinal); number of invariants of type $P_n \partial_n (\eta_i \eta_j \eta_k \eta_l)$ is 5 (transverse); in total, it is 20.

	Number of invariants		
	39		
	$\partial_m (\eta_i \eta_j \eta_k \eta_l)$	$\eta_i \eta_j \partial_m (\eta_k \eta_l) - \eta_k \eta_l \partial_m (\eta_i \eta_j)$	$\eta_i \eta_j \partial_m (\eta_k \eta_l)$
	20	7	12
$P_i \partial_i$	15	0	6
$P_i \partial_j$	5	7	6

ant type and correspond to the last two rows in the tables. The invariants V are Lifshitz-like. The invariants are

$$U_{T1} = P_z \partial_y [(\eta_1^2 + \eta_2^2 - \eta_3^2 - \eta_4^2)(\eta_5^2 + \eta_6^2)], \quad (\text{A4})$$

$$U_{T2} = P_y \partial_x [(\eta_1^2 + \eta_2^2 - \eta_3^2 - \eta_4^2)(\eta_5^2 + \eta_6^2)] + P_z \partial_x [(\eta_1^2 + \eta_2^2 + \eta_3^2 + \eta_4^2)(\eta_5^2 + \eta_6^2)], \quad (\text{A5})$$

$$U_{T3} = P_x \partial_y [(\eta_1^2 + \eta_2^2 - \eta_3^2 - \eta_4^2)(\eta_5^2 + \eta_6^2)], \quad (\text{A6})$$

$$U_{T4} = P_y \partial_x (\eta_1^2 \eta_2^2 - \eta_3^2 \eta_4^2) + P_x \partial_y (\eta_1^2 \eta_2^2 - \eta_3^2 \eta_4^2) + P_z \partial_x (\eta_5^2 \eta_6^2), \quad (\text{A7})$$

$$U_{T5} = P_y \partial_x (\eta_1^4 + \eta_2^4 - \eta_3^4 - \eta_4^4) + P_x \partial_y (\eta_1^4 + \eta_2^4 - \eta_3^4 - \eta_4^4) + P_z \partial_x (\eta_5^4 + \eta_6^4), \quad (\text{A8})$$

$$U_{L1} = P_y \partial_y (\eta_5^2 \eta_6^2), \quad (\text{A9})$$

$$U_{L2} = P_y \partial_y (\eta_5^4 + \eta_6^4), \quad (\text{A10})$$

$$U_{L3} = P_y \partial_y [(\eta_1^2 + \eta_2^2 + \eta_3^2 + \eta_4^2)(\eta_5^2 + \eta_6^2)], \quad (\text{A11})$$

$$U_{L4} = P_x \partial_x [(\eta_1^2 + \eta_2^2 + \eta_3^2 + \eta_4^2)(\eta_5^2 + \eta_6^2)], \quad (\text{A12})$$

$$U_{L5} = P_x \partial_x (\eta_1 \eta_2 \eta_3 \eta_4) - P_y \partial_y (\eta_1 \eta_2 \eta_3 \eta_4), \quad (\text{A13})$$

$$U_{L6} = P_x \partial_x (\eta_2^2 \eta_3^2 + \eta_1^2 \eta_4^2) + P_y \partial_y (\eta_2^2 \eta_3^2 + \eta_1^2 \eta_4^2), \quad (\text{A14})$$

$$U_{L7} = P_x \partial_x (\eta_1^2 \eta_3^2 + \eta_2^2 \eta_4^2) + P_y \partial_y (\eta_1^2 \eta_3^2 + \eta_2^2 \eta_4^2), \quad (\text{A15})$$

TABLE III. Total number of invariants under assumptions $\partial_z = 0$, $\eta_i = 0$, $i = 7, \dots, 12$. The invariant forms and their count are indicated, e.g., in the first column: number of invariants of type $P_m \partial_m (\eta_i \eta_j \eta_k \eta_l)$ is 9 (longitudinal); number of invariants of type $P_n \partial_n (\eta_i \eta_j \eta_k \eta_l)$ is 5 (transverse); in total, it is 14.

	Number of invariants ($\partial_z = 0$, $\eta_i = 0$, $i = 7, \dots, 12$)		
	25		
	$\partial_m (\eta_i \eta_j \eta_k \eta_l)$	$\eta_i \eta_j \partial_m (\eta_k \eta_l) - \eta_k \eta_l \partial_m (\eta_i \eta_j)$	$\eta_i \eta_j \partial_m (\eta_k \eta_l)$
	14	3	8
$P_i \partial_i$	9	0	2
$P_i \partial_j$	5	3	6

$$U_{L8} = P_x \partial_x (\eta_1^2 \eta_2^2 + \eta_3^2 \eta_4^2 + \eta_5^2 \eta_6^2) + P_y \partial_y (\eta_1^2 \eta_2^2 + \eta_3^2 \eta_4^2), \quad (\text{A16})$$

$$U_{L9} = P_x \partial_x (\eta_1^4 + \eta_2^4 + \eta_3^4 + \eta_4^4 + \eta_5^4 + \eta_6^4) + P_y \partial_y (\eta_1^4 + \eta_2^4 + \eta_3^4 + \eta_4^4), \quad (\text{A17})$$

$$V_{T1} = P_y [\eta_3 \eta_4 \partial_x (\eta_1 \eta_2) - \eta_1 \eta_2 \partial_x (\eta_3 \eta_4)] + P_x [\eta_1 \eta_2 \partial_y (\eta_3 \eta_4) - \eta_3 \eta_4 \partial_y (\eta_1 \eta_2)], \quad (\text{A18})$$

$$V_{T2} = P_y [\eta_1^2 \partial_x (\eta_4^2) - \eta_4^2 \partial_x (\eta_1^2) + \eta_2^2 \partial_x (\eta_3^2) - \eta_3^2 \partial_x (\eta_2^2)] + P_x [\eta_1^2 \partial_y (\eta_4^2) - \eta_4^2 \partial_y (\eta_1^2) + \eta_2^2 \partial_y (\eta_3^2) - \eta_3^2 \partial_y (\eta_2^2)], \quad (\text{A19})$$

$$V_{T3} = P_y [\eta_1^2 \partial_x (\eta_3^2) - \eta_3^2 \partial_x (\eta_1^2) + \eta_2^2 \partial_x (\eta_4^2) - \eta_4^2 \partial_x (\eta_2^2)] + P_x [\eta_1^2 \partial_y (\eta_3^2) - \eta_3^2 \partial_y (\eta_1^2) + \eta_2^2 \partial_y (\eta_4^2) - \eta_4^2 \partial_y (\eta_2^2)], \quad (\text{A20})$$

$$W_{T1} = P_z (\eta_1^2 + \eta_2^2 - \eta_3^2 - \eta_4^2) \partial_y (\eta_5^2 + \eta_6^2), \quad (\text{A21})$$

$$W_{T2} = P_y (\eta_5^2 + \eta_6^2) \partial_x (\eta_1^2 + \eta_2^2 - \eta_3^2 - \eta_4^2) + P_z (\eta_1^2 + \eta_2^2 + \eta_3^2 + \eta_4^2) \partial_x (\eta_5^2 + \eta_6^2), \quad (\text{A22})$$

$$W_{T3} = P_z (\eta_5^2 + \eta_6^2) \partial_y (\eta_1^2 + \eta_2^2 - \eta_3^2 - \eta_4^2), \quad (\text{A23})$$

$$W_{T4} = P_x (\eta_5^2 + \eta_6^2) \partial_y (\eta_1^2 + \eta_2^2 - \eta_3^2 - \eta_4^2), \quad (\text{A24})$$

$$W_{T5} = P_z (\eta_5^2 + \eta_6^2) \partial_x (\eta_1^2 + \eta_2^2 + \eta_3^2 + \eta_4^2) + P_y (\eta_1^2 + \eta_2^2 - \eta_3^2 - \eta_4^2) \partial_x (\eta_5^2 + \eta_6^2), \quad (\text{A25})$$

$$W_{T6} = P_x (\eta_1^2 + \eta_2^2 - \eta_3^2 - \eta_4^2) \partial_y (\eta_5^2 + \eta_6^2), \quad (\text{A26})$$

$$W_{L1} = P_y (\eta_5^2 + \eta_6^2) \partial_y (\eta_1^2 + \eta_2^2 + \eta_3^2 + \eta_4^2), \quad (\text{A27})$$

$$W_{L2} = P_y (\eta_1^2 + \eta_2^2 + \eta_3^2 + \eta_4^2) \partial_y (\eta_5^2 + \eta_6^2). \quad (\text{A28})$$

-
- [1] G. Pilania, D. Q. Tan, Y. Cao, V. S. Venkataramani, Q. Chen, and R. Ramprasad, *Ab initio* study of antiferroelectric PbZrO₃ (001) surfaces, *J. Mater. Sci.* **44**, 5249 (2009).
- [2] J. Íñiguez, M. Stengel, S. Prosandeev, and L. Bellaiche, First-principles study of the multimode antiferroelectric transition in PbZrO₃, *Phys. Rev. B* **90**, 220103(R) (2014).
- [3] S. Amisi, *Ab initio* investigation in PbZrO₃ antiferroelectric: structural and vibrational properties, *Eur. Phys. J. Plus* **136**, 653 (2021).
- [4] E. A. Kotomin, S. Piskunov, Y. F. Zhukovskii, R. I. Eglitis, A. Gopejenko, and D. E. Ellis, The electronic properties of an oxygen vacancy at ZrO₂-terminated (001) surfaces of a cubic PbZrO₃: computer simulations from the first principles, *Phys. Chem. Chem. Phys.* **10**, 4258 (2008).
- [5] R. I. Eglitis, J. Purans, J. Gabrusenoks, A. I. Popov, and R. Jia, Comparative *ab initio* calculations of ReO₃, SrZrO₃, BaZrO₃, PbZrO₃ and CaZrO₃ (001) surfaces, *Crystals* **10**, 745 (2020).
- [6] R. I. Eglitis and A. I. Popov, *Ab initio* Calculations of Bulk and (001) Surface F-centers in ABO₃ Perovskites, in *2021 IEEE 12th International Conference on Electronics and Information Technologies (ELIT)* (IEEE, Piscataway, NJ, 2021), pp. 283–286.
- [7] S. Van Aert, S. Turner, R. Delville, D. Schryvers, G. Van Tendeloo, and E. K. Salje, Direct observation of ferrielectricity at ferroelastic domain boundaries in CaTiO₃ by electron microscopy, *Adv. Mater.* **24**, 523 (2012).
- [8] H. Yokota, H. Usami, R. Haumont, P. Hicher, J. Kaneshiro, E. K. H. Salje, and Y. Uesu, Direct evidence of polar nature of ferroelastic twin boundaries in CaTiO₃ obtained by second harmonic generation microscope, *Phys. Rev. B* **89**, 144109 (2014).
- [9] H. Yokota, S. Niki, R. Haumont, P. Hicher, and Y. Uesu, Polar nature of stress-induced twin walls in ferroelastic CaTiO₃, *AIP Adv.* **7**, 085315 (2017).
- [10] E. K. H. Salje, O. Aktas, M. A. Carpenter, V. V. Laguta, and J. F. Scott, Domains within Domains and Walls within Walls: Evidence for Polar Domains in Cryogenic SrTiO₃, *Phys. Rev. Lett.* **111**, 247603 (2013).
- [11] S. Lei, H. Fan, J. Fang, X. Ren, L. Ma, and H. Tian, Unusual devisable high-performance perovskite materials obtained by engineering in twins, domains, and antiphase boundaries, *Inorg. Chem. Front.* **5**, 568 (2018).
- [12] G. Nataf, M. Guennou, J. Gregg, D. Meier, J. Hlinka, E. Salje, and J. Kreisel, Domain-wall engineering and topological defects in ferroelectric and ferroelastic materials, *Nat. Rev. Phys.* **2**, 634 (2020).
- [13] G. Catalan, J. Seidel, R. Ramesh, and J. F. Scott, Domain wall nanoelectronics, *Rev. Mod. Phys.* **84**, 119 (2012).
- [14] E. K. Salje, M. Alexe, S. Kustov, M. C. Weber, J. Schiemer, G. F. Nataf, and J. Kreisel, Direct observation of polar tweed in LaAlO₃, *Sci. Rep.* **6**, 27193 (2016).
- [15] H. Yokota, N. Hasegawa, M. Glazer, E. Salje, and Y. Uesu, Direct evidence of polar ferroelastic domain boundaries in semiconductor BiVO₄, *Appl. Phys. Lett.* **116**, 232901 (2020).
- [16] Y. Gu, M. Li, A. N. Morozovska, Y. Wang, E. A. Eliseev, V. Gopalan, and L.-Q. Chen, Flexoelectricity and ferroelectric domain wall structures: phase-field modeling and DFT calculations, *Phys. Rev. B* **89**, 174111 (2014).
- [17] A. Schiaffino and M. Stengel, Macroscopic Polarization from Antiferrodistortive Cycloids in Ferroelastic SrTiO₃, *Phys. Rev. Lett.* **119**, 137601 (2017).
- [18] X.-K. Wei, A. K. Tagantsev, A. Kvasov, K. Roleder, C.-L. Jia, and N. Setter, Ferroelectric translational antiphase boundaries in nonpolar materials, *Nat. Commun.* **5**, 3031 (2014).
- [19] V. Janovec and J. Přívratká, Domain structures, in *International Tables for Crystallography* (International Union of Crystallography, 2006) pp. 449–505.
- [20] V. Janovec, W. Schranz, H. Warhanek, and Z. Zikmund, Symmetry analysis of domain structure in KSCN crystals, *Ferroelectrics* **98**, 171 (1989).

- [21] Y. Ishibashi and V. Dvořák, Domain walls in improper ferroelectrics, *J. Phys. Soc. Jpn.* **41**, 1650 (1976).
- [22] A. A. Bullbich and Y. M. Gufan, Phase transitions in domain walls, *Ferroelectrics* **98**, 277 (1989).
- [23] B. Houchmandzadeh, J. Lajzerowicz, and E. Salje, Order parameter coupling and chirality of domain walls, *J. Phys.: Condens. Matter* **3**, 5163 (1991).
- [24] A. K. Tagantsev, E. Courtens, and L. Arzel, Prediction of a low-temperature ferroelectric instability in antiphase domain boundaries of strontium titanate, *Phys. Rev. B* **64**, 224107 (2001).
- [25] E. B. Sonin and A. K. Tagantsev, Structure and phase transitions in antiphase boundaries of improper ferroelectrics, *Ferroelectrics* **98**, 291 (1989).
- [26] A. N. Morozovska, E. A. Eliseev, M. D. Glinchuk, L.-Q. Chen, and V. Gopalan, Interfacial polarization and pyroelectricity in antiferrodistortive structures induced by a flexoelectric effect and rotostriction, *Phys. Rev. B* **85**, 094107 (2012).
- [27] A. K. Tagantsev, K. Vaideeswaran, S. B. Vakhrushev, A. V. Filimonov, R. G. Burkovsky, A. Shaganov, D. Andronikova, A. I. Rudskoy, A. Q. R. Baron, H. Uchiyama, D. Chernyshov, A. Bosak, Z. Ujma, K. Roleder, A. Majchrowski, J.-H. Ko, and N. Setter, The origin of antiferroelectricity in PbZrO_3 , *Nat. Commun.* **4**, 2229 (2013).
- [28] W. Schranz, I. Rychetsky, and J. Hlinka, Polarity of domain boundaries in nonpolar materials derived from order parameter and layer group symmetry, *Phys. Rev. B* **100**, 184105 (2019).
- [29] W. Schranz, C. Schuster, A. Tröster, and I. Rychetsky, Polarization of domain boundaries in SrTiO_3 studied by layer group and order-parameter symmetry, *Phys. Rev. B* **102**, 184101 (2020).
- [30] W. Schranz, A. Tröster, and I. Rychetsky, Contributions to polarization and polarization switching in antiphase boundaries of SrTiO_3 and PbZrO_3 , *J. Appl. Phys.* **128**, 194101 (2020).
- [31] X.-K. Wei, C.-L. Jia, K. Roleder, and N. Setter, Polarity of translation boundaries in antiferroelectric PbZrO_3 , *Mater. Res. Bull.* **62**, 101 (2015).
- [32] T. Ma, Z. Fan, X. Tan, and L. Zhou, Atomically resolved domain boundary structure in lead zirconate-based antiferroelectrics, *Appl. Phys. Lett.* **115**, 122902 (2019).
- [33] H. Fujishita and S. Hoshino, A study of structural phase transitions in antiferroelectric PbZrO_3 by neutron diffraction, *J. Phys. Soc. Jpn.* **53**, 226 (1984).
- [34] H. Fujishita and S. Katano, Re-examination of the antiferroelectric structure of PbZrO_3 , *J. Phys. Soc. Jpn.* **66**, 3484 (1997).
- [35] K. Momma and F. Izumi, VESTA3 for three-dimensional visualization of crystal, volumetric and morphology data, *J. Appl. Crystallogr.* **44**, 1272 (2011).
- [36] J. Hlinka, T. Ostapchuk, E. Buixaderas, C. Kadlec, P. Kuzel, I. Gregora, J. Kroupa, M. Savinov, A. Klic, J. Drahoš, I. Etxebarria, and J. Dec, Multiple Soft-Mode Vibrations of Lead Zirconate, *Phys. Rev. Lett.* **112**, 197601 (2014).
- [37] K. M. Rabe, Antiferroelectricity in oxides: a reexamination, in *Functional Metal Oxides*, edited by S. B. Ogale, T. V. Venkatesan, and M. G. Blamire (John Wiley & Sons, Ltd, 2013), Chap. 7, pp. 221–244.
- [38] P. Tolédano and D. D. Khalyavin, Symmetry-determined antiferroelectricity in PbZrO_3 , NaNbO_3 , and PbHfO_3 , *Phys. Rev. B* **99**, 024105 (2019).
- [39] M. I. Aroyo, A. Kirov, C. Capillas, J. M. Perez-Mato, and H. Wondratschek, Bilbao Crystallographic Server. II. Representations of crystallographic point groups and space groups, *Acta Crystallogr., Sect. A* **62**, 115 (2006).
- [40] The translational domain states with respect to the oxygen octahedra rotations ϕ are not considered in this paper.
- [41] A. Kvasov, A. K. Tagantsev, and N. Setter, Structure and pressure-induced ferroelectric phase transition in antiphase domain boundaries of strontium titanate from first principles, *Phys. Rev. B* **94**, 054102 (2016).